

Electronic Localization in CaVO_3 Films via Bandwidth Control

Daniel E. McNally¹, Xingye Lu¹, Jonathan Pellicciari^{1,†}, Sophie Beck², Marcus Dantz¹, Muntaser Naamneh¹, Tian Shang^{1,3}, Marisa Medarde⁴, Christof W. Schneider⁵, Vladimir N. Strocov¹, Ekaterina V. Pomjakushina⁴, Claude Ederer², Milan Radovic^{1#}, and Thorsten Schmitt^{1*}

¹ Photon Science Division, Paul Scherrer Institut, CH-5232 Villigen PSI, Switzerland.

² Materials Theory, ETH Zurich, Wolfgang-Pauli Strasse 27, CH-8093 Zurich, Switzerland

³ Institute of Condensed Matter Physics, Ecole Polytechnique Federale de Lausanne (EPFL), CH-1015 Lausanne, Switzerland

⁴Laboratory for Scientific Developments and Novel Materials, Paul Scherrer Institut, CH-5232 Villigen PSI, Switzerland

⁵Laboratory for Multiscale Materials Experiments, Paul Scherrer Institut, CH-5232 Villigen PSI, Switzerland

[†] Current address: Department of Physics, Massachusetts Institute of Technology, Cambridge, Massachusetts 02139, USA

* thorsten.schmitt@psi.ch

milan.radovic@psi.ch

Key Words: transition metal oxides, thin films, resonant inelastic X-ray scattering, X-ray absorption spectroscopy, electronic structure, metal-insulator transition

Abstract:

Understanding and controlling the electronic structure of thin layers of quantum materials is a crucial first step towards designing heterostructures where new phases and phenomena, including the metal-insulator transition (MIT), emerge. Here, we demonstrate control of the MIT via tuning electronic bandwidth and local site environment through selection of the number of atomic layers deposited. We take CaVO_3 , a correlated metal in its bulk form that has only a single electron in its V^{4+} 3d manifold, as a representative example. We find that thick films and ultrathin films (≤ 6 unit cells, u.c.) are metallic and insulating, respectively, while a 10 u.c. CaVO_3 film exhibits a clear thermal MIT. Our combined X-ray absorption spectroscopy and resonant inelastic x-ray scattering (RIXS) study reveals that the thickness-induced MIT is triggered by electronic bandwidth reduction and local moment formation from V^{3+} ions, that are both a consequence of the thickness confinement. The thermal MIT in our 10 u.c. CaVO_3 film exhibits similar changes in the RIXS response to that of the thickness-induced MIT in terms of reduction of bandwidth and V 3d – O 2p hybridization.

Introduction

Deposition methods with unit cell thickness precision enable new approaches to control the degree of electronic localization in quantum materials. For instance, epitaxial strain changes the lattice parameters altering the potential landscape of the electrons, dimensionality tunes the electronic bandwidth and interfacing provides a charge reservoir. Thickness-dependent metal-insulator transitions (MIT) in thin films have been widely reported in recent years in a broad swathe of correlated 3d and 5d transition metal oxides [1-7]. Understanding and controlling the electronic

structure of these quantum materials is a critical first step toward designing heterostructures where new emergent phases and phenomena, including MIT, have been widely predicted [8, 9]. The focus of our interest is to resolve the nature of the thickness-induced MIT, therefore, in this work we consider CaVO_3 as a model system.

Bulk CaVO_3 with a formal valence shell configuration of $V3d^1$ (V^{4+} oxidation state) is a paramagnetic metal with enhanced Sommerfeld-Wilson and Kadowaki-Woods ratios suggesting electronic correlations are important [10]. However, as is often the case for metals, neither moderate doping nor pressure induce insulating or magnetic ground states [11,12]. In contrast to the bulk, enhanced electron correlation strength and a MIT have recently been reported for CaVO_3 films of 20 unit cells (u.c.) or less [6,13]. While these discoveries are promising for technological applications such as transparent conductors [13] and MottFETs [14,15], a complete understanding of the MIT in CaVO_3 has, until now, remained elusive.

Figure 1 illustrates that electronic bandwidth can control the degree of electron localization in $3d^1$ perovskites RXO_3 . In the example presented in the top panels, applicable for bulk-like materials, when the orthorhombic distortion is increased the bandwidth decreases by up to 40 % and a MIT occurs [16]. However, realising this MIT requires the substitution of both R and X ions making it very difficult to continuously control in practice. In our work presented here we show that the bandwidth can be controlled continuously by up to 40 % in CaVO_3 simply by choosing the number of atomic layers deposited on a SrTiO_3 substrate as summarized in the bottom panels of Figure 1 and outlined in detail in the rest of this work.

Results

Metal-insulator transition in thin film CaVO_3 .

Figure 2a presents electrical resistance as a function of temperature for our CaVO_3 and SrVO_3 thin films grown by pulsed laser deposition (PLD) on SrTiO_3 (100) substrates. The film thicknesses and surface ordering were routinely monitored with single-layer accuracy by reflection high-energy electron diffraction (RHEED), see Fig. 1 in S.I.. For the thinner films (15 u.c., 10 u.c., 6 u.c., 4 u.c. CaVO_3) a thin 2 nm SrTiO_3 overlayer was deposited to protect against environmental (in air) degradation upon removal from PLD chamber. The thick 50 u.c. films are metallic at all temperatures, like bulk CaVO_3 and SrVO_3 [10,17]. When the CaVO_3 (CVO) film thickness is reduced a MIT occurs. The 15 u.c. and 10 u.c. films undergo a MIT at 160 K and 220 K respectively while the 6 u.c. and 4 u.c. films are insulating at all temperatures (the 4 u.c. film was too insulating to be measured using our setup). The overall behaviour is similar to that previously reported for CaVO_3 films [6]. Comparison of RHEED patterns recorded at room temperature after deposition of 15 u.c. CVO (metallic at room temperature) and 6 u.c. CVO (insulating at room temperature) films suggests structural transitions (possibly octahedral rotation) to play a role in the thickness-induced MIT (See S.I. Fig 3). We emphasize that this structural reconstruction was only observed for the very thin CaVO_3 film of 6 u.c. thickness that was capped by a 2 nm (5. u.c.) SrTiO_3 over-layer (compare Fig. 1 and Fig. 3 in S.I.). We ascribe an important role to the SrTiO_3 over-layer in inducing and/or stabilizing this structural reconstruction.

X-ray absorption (XAS) at the V $L_{2,3}$ edges presented in Figure 2b reveals an evolution from broad d-bands and large valence fluctuations in metallic thick films of CaVO_3 to a more localized 3d character in the thinner insulating films. XAS of the thick metallic 50 u.c. film (red line) is similar to that of a CaVO_3 single crystal (brown), as well as a 50 u.c. SrVO_3 film (dashed black). These spectra

are not well reproduced by multiplet calculations because of the itinerant character of the 3d electrons [18]. With reduced film thickness the XAS spectra become sharper, the L_3 peak energy is reduced by ~ 0.5 eV, a shoulder appears on the L_3 peak and a new peak is found in the dip between L_3 and L_2 peaks. These new peaks are commonly observed in insulating VO_2 (V^{4+} , dashed grey) and V_2O_3 (V^{3+}) compounds (dashed magenta) [19]. In particular, XAS of the thinner most insulating CaVO_3 films (6 u.c. and 4 u.c.) is similar to that reported for $\text{Y}_{1-x}\text{Ca}_x\text{VO}_3$ ($x \geq 0.6$) that contains both V^{4+} and V^{3+} character [18]. The increase in V^{3+} results from charge redistribution in the thinner films and is consistent with a reduced Madelung potential and hence reduced V-O covalency across the MIT. The sharpening of the $L_{2,3}$ peaks across the MIT reflects a reduction in the bandwidth of the upper Hubbard band. XAS of the 10 u.c. film in the high temperature metallic state is presented as a dashed blue curve in Figure 2b. A broadening of the spectral features is observed with respect to the low temperature insulating state but the overall response is still different from that of the metallic thick 50 u.c. CaVO_3 film. We undertook a series of resonant inelastic x-ray scattering (RIXS) measurements to investigate further the change in the electronic excitations across the thickness-induced and thermal MIT.

Control of electronic bandwidth in CaVO_3 .

Figure 3 presents RIXS intensity maps of energy transfer versus incident energy at $T = 20$ K across the V L_3 edge. First, we discuss the energy map for the 50 u.c. SrVO_3 and CaVO_3 films presented in the panels 3a and 3b. Three fluorescence features [20], where the energy transfer disperses linearly with incident energy, are evident at higher energy transfers (marked as F1, F2, F3 in Figure 3c). These spectral signatures have been observed previously for single crystal CaVO_3 and were assigned to, for decreasing energy transfer, a hybridized V-O band (F3), an inter-band transition involving the lower Hubbard band (F2), and an intra-band transition involving a quasiparticle-like

band (F1) [21]. Furthermore, we observe several new Raman-like modes where the energy transfer is independent of incident energy. We assign the intense Raman mode (R1) located at ~ 0.3 eV (0.5 eV for SrVO₃) to electron-hole pair excitations [22]. The Raman-like scattering at higher energy transfers (R2) is assigned to crystal-field excitations. The assignment of fluorescence and Raman peaks is illustrated in a schematic representation of occupied and unoccupied density of states in Figure 3e.

The RIXS response undergoes a large change as we traverse the thickness-induced MIT in CaVO₃. RIXS maps for insulating 10 u.c. and 4 u.c. films are presented in Figure 3c,d. Our first observation is that the spectral weight in the fluorescence features has decreased relative to the spectral weight in the Raman modes as the film thickness is decreased. This transfer of spectral weight from band to localised excitations is expected as we move from metallic to insulating behaviour. We also observe that the measured peaks become sharper and there is a reduction of the bandwidth of these electronic excitations. The reduced bandwidth of electronic excitations measured across the MIT in our RIXS experiment on CaVO₃ is similar to the reduced bandwidth measured using angle-resolved photoemission (ARPES) across the thickness-induced MIT in thin films of another vanadate, SrVO₃, that was ascribed to a dimensional crossover below 3-4 u.c. [5]. In the case of CaVO₃ reported here the crossover occurs at a larger thickness of 10 u.c. suggesting that both strain and dimensionality influence the MIT. Indeed it has been shown that strain can substantially affect the MIT in other systems, such as NdNiO₃ [23].

We quantify the reduction in the bandwidth of the electronic excitations by fitting the data and present the corresponding line cuts and fit results in Figure 4. The thickness-dependence of the low energy Raman-like RIXS peak that we assign to electron-hole pair excitations [20,22,24] is presented in Figure 4a. The elastic line has been subtracted and the corresponding fits are

presented in supplementary information (S.I.). We extract from our fits the bandwidth and energy scale of the electron-hole pair excitations and present these results in Figure 4c (bottom). The bandwidth is gradually reduced from 0.73 eV in the SrVO₃ 50 u.c. film to 0.63 eV in the CaVO₃ 50 u.c. film to 0.38 eV in the insulating 6 u.c. and 4 u.c. CaVO₃ films. The peak energy exhibits a large jump from 0.5 eV to 0.3 eV from SrVO₃ 50 u.c. to CaVO₃ 50 u.c. and then is gradually reduced to nearly 0.2 eV in the insulating 6 u.c. and 4 u.c. films.

In Figure 4b, 4c (top) we present line cuts and fit results for the fluorescence features F1 and F2 that are band excitations. We illustrate the origin of the F1 and F2 features in Figure 3 (bottom) and assign F1 to intra-band excitations involving a quasiparticle-like band and F2 to inter-band excitations involving the lower Hubbard band [21]. The separation between these two RIXS peaks is ~ 1.8 eV, the same energy separation as the low-energy optical conductivity peaks that were also interpreted as originating from intra- and inter-band excitations. Further support for this interpretation is provided by photoemission spectra that reveal a lower Hubbard band at 1.8 eV below the Fermi level [25]. The total bandwidth of our two measured RIXS peaks, determined from the first derivative of the spectra (shown in S.I.), scales with the bandwidth of the V 3d valence band [19]. Figure 4c (top) presents the results of this analysis. The total bandwidth displays a sharp drop between the metallic 50 u.c. CaVO₃ film (= 4 eV) and the 15 u.c. CaVO₃ film (= 3.5 eV) that is on the verge of being insulating (see Figure 2a). The bandwidth continues to decrease gradually to 3.2 eV in the most insulating 4 u.c. CaVO₃ film. A guide for the eye in Figure 4b shows the reduction in the separation between intra- and inter-band peaks, consistent with the bandwidth reduction extracted from our derivative analysis. For the 4 u.c. film the relative spectral weight in the intra-band peak substantially decreases with respect to the inter-band peak (compared to the 50 u.c. CaVO₃ film) as the spectral weight is transferred away from the valence band maximum. However,

there is still weight in the intra-band peak even in the insulating phase indicating metallic puddles are still present even in the insulating phase [26].

Local moment formation in CaVO₃ films.

There are several Raman-like peaks marked as R2 in Figure 3 and we present line cuts through this region for different film thicknesses in Figure 5 (left). In the thick metallic 50 u.c. SrVO₃ film, that is nominally a perfect cubic structure with no octahedral tilting and formal valence band configuration of V 3d¹, we observe a broad peak centered around 1.9 eV, a similar energy scale to the t_{2g}-e_g excitations found near 1.7 eV in the insulator YVO₃ with a valence electron configuration of V 3d² [27]. For the 50 u.c. CaVO₃ film, that has a small orthorhombic distortion and octahedral tilting, we find a large broadening and nearly flat distribution of spectral weight. A three peaks structure is measured in the 15 u.c. CaVO₃ film and these peaks continue to sharpen in the insulating 10 u.c., 6 u.c. and 4 u.c. CaVO₃ films (Figure 5 (left)). There are two possible explanations for this reconstruction: strain-induced changes in bond lengths or the formation of local magnetic moments [27]. The effect of epitaxial strain is larger in the thinner films but strain effects are expected to lift the degeneracy of the t_{2g} and e_g states by only a small amount (~ 100 meV) [15] compared to the large effect reported here. The additional peaks are therefore a clear signature of local moment formation from V³⁺ ions allowing spin flips from a t_{2g}² high spin S=1 ground state configuration to configurations involving S=0 and the e_g level [27]. We already have evidence that V³⁺ ions are present in thinner CaVO₃ films from our XAS as described earlier and thus we can attribute the additional peak near 1 eV to a local spin flipping t_{2g}² S=0 transition at twice the Hund's coupling energy 2J_H using the notation of ref. [27]. The additional peak near 2.6 eV is also captured by several overlapping local excitations on the V³⁺ ion, namely by transitions to t_{2g}² with S=0 of higher crystal field symmetry and to t_{2g}¹e_g¹ with S=1 or S=0 [27]. The formation of a local moment

in insulating ultra-thin CaVO_3 films starting from a bulk-like non-magnetic thin film is a dramatic effect, resulting from a control of electronic bandwidth and charge redistribution.

Thermal MIT in 10 u.c. CaVO_3 film and the role of V-O hybridization.

Now we draw the attention to the MIT which occurs below 220 K in the 10 u.c. CaVO_3 film (see Figure 2a). We present in Figure 6 the RIXS intensity as a function of energy transfer for the 10 u.c. film in the room temperature metallic phase (at 300 K) and at 20 K, deep in the insulating phase. The change in the RIXS response across the thermal MIT is qualitatively similar to the change for the thickness-induced MIT (see also Fig. 4c): the bandwidth of the electron-hole pair excitation decreases by ca. 15% along with a small softening of the peak position (Figure 6a), the crystal field levels sharpen (Figure 6b), and the total bandwidth near the valence band maximum decreases by about 5% (Figure 6c). In addition, we can quantitatively comment on the relative strength of the high-energy V 3d - O 2p hybridization band shown in Figure 6d: the intensity of this peak is reduced by 10% in the insulating phase. The reduced V-O hybridization across the thermal MIT is comparable to the relative suppression of weight in this hybridized band upon entering the thickness-induced insulating state as shown in Figure 3 (also see line cuts in S.I. Fig. 7). Thus, the same trend of reduced electronic bandwidth and reduced V-O hybridization is measured in both thermal and thickness-induced MIT, with the effects on the thickness-induced MIT being a factor 2-3 larger.

Discussion

The large reduction of bandwidth in our CaVO_3 films is comparable to that realized in the $3d^1$ perovskite series SrVO_3 - CaVO_3 - LaTiO_3 - YTiO_3 as shown in Figure 1. The MIT in the latter case is

attributed to an increased orthorhombic distortion, and local moment formation, as the cation size is changed [16]. Obviously control of this MIT is chemically difficult as it involves substituting two elements, illustrating the usefulness of the additional parameter space enabled by thin film synthesis methods.

We can understand our results by comparing the experimental spectra for the thermal- and thickness-induced MIT. In the thermal MIT case at constant film thickness we still need to consider the epitaxial strain. Strain will induce changes in the V-O bond lengths and V-O overlap/hybridization as experimentally observed in other $3d^1$ perovskites [28]. We thus propose that a structural and/or magnetic transition is driving the thermal MIT in our 10 u.c. CaVO_3 film as observed in e.g. nickelate films such as NdNiO_3 [23]. This proposal is supported by the data presented in Figure 6b that shows a sharpening of crystal field excitations across the thermal MIT. For the thinner CaVO_3 films, the electron-hole bandwidth (see Figure 1 and 4 c,d) is sharply reduced moving from 10 u.c. to 6 u.c. and 4 u.c. films. Additionally XAS reveals increasing V $3d^2$ contributions (Figure 2b) and the crystal field excitations become much sharper for the thickness-induced MIT (Figure 5).

The increased contribution from V^{3+} ions in the thinner films stems from charge redistribution and is connected to a reduced V-O covalence across the MIT. The reduction of the V 3d bandwidth is driven by a structural reconstruction accompanied by octahedral rotation, that is thereby also changing the V-O hybridization, manifested in an abrupt change of the RHEED patterns of the ultra-thin capped films. In this sense the “electronic localization and bandwidth reduction” as well as the “increase of V^{3+} contributions” are a consequence of the thickness confinement. Oxygen vacancies generated during the growth of CVO films might partially contribute to V^{3+} states, but their amount, in principle, should scale with the film thickness. However, 50 u.c. CVO film does not show more

V^{3+} signature in the spectra than thinner CVO films suggesting no significant influence of oxygen vacancies on the properties of the studied CVO films.

The combined effects of charge redistribution, confinement, as well as strain are important in the ultrathin CaVO_3 films [29]. Based on the results presented here it is difficult to distinguish which of these effects is the main player driving the thickness-induced MIT. However, we note that the MIT appears to be significantly more complex than the dimensional crossover-driven MIT reported in ultrathin SrVO_3 films using angle-resolved photoemission spectroscopy [5].

Our experiments reveal a bandwidth-driven MIT in CaVO_3 films as a function of both thickness and temperature where strain, dimensionality and charge redistribution contribute. A reduced V-O hybridization in the insulating state reveals that the MIT is of Mott-Hubbard type where a d-d gap is opened by a strong Coulomb interaction U between electrons [30]. The sharp thermal MIT observed in our 10 u.c. CaVO_3 film should stimulate future work on this model system. Our results are promising for the future of the field of correlated electronics showing that while increased disorder can be present in ultra-thin films, it does not inhibit the Mott physics and related spin or charge ordering. However, we want to emphasise the radical changes in electronic structure that can occur in films of reduced dimensionality, and the importance of including these effects in the rational design of new quantum materials.

Methods

Experimental details.

X-ray absorption (XAS) and resonant inelastic x-ray scattering (RIXS) experiments were carried out at the ADRESS beamline of the Swiss Light Source at the Paul Scherrer Institut [31]. All measurements were performed at grazing incidence with the x-rays incident at 15° with respect to the sample surface and with σ or π polarisation. The scattering angle was fixed at 130° . We set the spectrometer [32] in the high throughput configuration using the 1500 lines per mm variable line spacing (VLS) spherical grating [33] as well as the newly installed CCD camera that provides sub-pixel spatial resolution [34]. The beamline exit slit was $20\ \mu\text{m}$. The setup yielded a total energy resolution (full width at half maximum FWHM) of around 60 meV.

Thin films of CaVO_3 and SrVO_3 were prepared on SrTiO_3 (100) and NdGaO_3 (110) substrates respectively by pulsed laser deposition (PLD). More information can be found in the supplementary information.

Data Availability

The datasets generated during and/or analysed during the current study are available from the corresponding authors on reasonable request.

Acknowledgements:

D.M.N. and T.S. thanks A. Georges (University of Geneva) for a helpful discussion. D.M.N. acknowledges helpful discussion and analytical tools from Eugenio Paris (PSI). The work at PSI is supported by the Swiss National Science Foundation through the NCCR MARVEL and the Sinergia network Mott Physics Beyond the Heisenberg Model (MPBH). Xingye Lu acknowledges financial support from the European Community's Seventh Framework Programme (FP7/20072013) under Grant agreement No. 290605 (Cofund; PSI-Fellow). J.P. and T.S. acknowledge financial support through the Dysenos AG by Kabelwerke Brugg AG Holding, Fachhochschule Nordwestschweiz, and the Paul Scherrer Institut. J.P. acknowledges financial support by the Swiss National Science Foundation Early Postdoc Mobility fellowship Project No. P2FRP2-171824. M.D. was partially funded by the Swiss National Science Foundation within the D-A-CH programme (SNSF Research Grant 200021L 141325).

Author Contributions:

M.R. and T.S. conceived the project. D.M.N., M.N., T.S., M.M., C.W.S., E.V.P. and M.R. grew and characterised the thin film samples. D.M.N., X.L., J.P., M.D., V.N.S., M.R. and T.S. carried out the XAS and RIXS experiments. D.M.N., M.R., and T.S. analysed the data. S.B. and C.E. carried out the DFT calculation. D.M.N., M.R., and T.S. wrote the paper with contributions from all authors.

Additional Information:

The authors declare no competing financial interests. Correspondence and requests should be addressed to T.S. (thorsten.schmitt@psi.ch) and M.R. (milan.radovic@psi.ch).

References

- [1] R. Scherwitzl, S. Gariglio, M. Gabay, P. Zubko, M. Gibert, and J.-M. Triscone, Metal-insulator transition in ultrathin LaNiO_3 films, *Phys. Rev. Lett.*, **106**, 246403 (2011).
- [2] P.D.C. King, H.I. Wei, Y.F. Nie, M. Uchida, C. Adamo, S. Zhu, X. He, I. Bozovic, D.G. Schlom, and K.M. Shen, Atomic-scale control of competing electronic phases in ultrathin LaNiO_3 , *Nat. Nano.*, **9**, 443 (2014).
- [3] Y. Feng, K. Jin, L. Gu, X. He, C. Ge, Q. Zhang, M. He, Q. Guo, Q. Wan, M. He, H. Lu, and G. Yang, Insulating phase at low temperature in ultrathin $\text{La}_{0.8}\text{Sr}_{0.2}\text{MnO}_3$ films, *Sci. Rep.*, **6**, 22382 (2016).
- [4] A. Biswas, K.-S. Kim, and Y.H. Yeong, Metal-insulator transitions and non-Fermi liquid behaviours in 5d perovskite iridates, *arXiv:1508.04929v2* (2016).
- [5] K. Yoshimatsu, T. Okabe, H. Kumigashira, S. Okamoto, S. Aizaki, A. Fujimori, and M. Oshima, Dimensional-crossover-driven metal-insulator transition in SrVO_3 ultrathin films, *Phys. Rev. Lett.*, **104**, 147601 (2010).
- [6] M. Gu, J. Laverock, B. Chen, K.E. Smith, S.A. Wolf, J. Lu, Metal-insulator transition induced in CaVO_3 thin films, *Journal of Applied Physics*, **113**, 133704 (2013).

- [7] M. Gu, S.A. Wolf, and J. Lu, Two-dimensional Mott insulators in SrVO₃ ultrathin films, *Adv. Mater. Interfaces*, 1, 1300126 (2014).
- [8] S.Y. Park, A. Kumar, and K.M. Rabe, Charge-order-induced ferroelectricity in LaVO₃/SrVO₃ superlattices, *Phys. Rev. Lett.*, 118, 087602 (2017).
- [9] J. Chakalian, J.W. Freeland, A.J. Millis, C. Panagopoulos, and J.M. Rondinelli, Colloquium: Emergent properties in plane view: Strong correlations at oxide interfaces, *Rev. Mod. Phys.*, 86, 1189-1202 (2014).
- [10] I.H. Inoue, O. Goto, H. Makino, N.E. Hussey, and M. Ishikawa, Bandwidth control in a perovskite-type 3d¹ correlated metal Ca_{1-x}Sr_xVO₃. I. Evolution of the electronic properties and effective mass, *Phys. Rev. B*, 58(8), 4372 (1998).
- [11] K. Maiti, N.Y. Vasanthacharya, and D.D. Sarma, Doping dependence of transport and magnetic properties in La_{1-x}Ca_xVO₃, *J. Phys. Cond. Mat.*, 9, 7507-7514 (1997).
- [12] J.-S. Zhou and J.B. Goodenough, Heterogeneous electronic structure in CaVO₃, *Phys. Rev. B*, 13393 (1996).
- [13] L. Zhang, Y. Zhou, L. Guo, W. Zhao, A. Barnes, H.-T. Zhang, C. Eaton, Y. Zheng, M. Brahlek, H.F. Haneef, N.J. Podraza, M.H.W. Chan, V. Gopalan, K.M. Rabe, and R. Engel-Herbert, Correlated metals at transparent conductors, *Nat. Mat.*, 15, 204210 (2016).
- [14] M. Nakano, K. Shibuya, D. Okuyama, T. Hatano, S. Ono, M. Kawasaki, Y. Iwasa, and Y. Tokura, Collective bulk carrier delocalization driven by electrostatic surface charge accumulation, *Nature*, 487, 459 (2012).

- [15] Z. Zhong, M. Wallerberger, J.M. Tomczak, C. Taranto, N. Parragh, A. Toschi, G. Sangiovanni, and K. Held, Electronics with correlated oxides: SrVO₃/SrTiO₃ as a Mott transistor, *Phys. Rev. Lett.*, 114, 246401 (2015).
- [16] E. Pavarini, S. Biermann, A. Poteryaev, A.I. Lichtenstein, A. Georges, and O.K. Andersen, Mott transition and suppression of orbital fluctuations in orthorhombic 3d1 perovskites, *Phys. Rev. Lett.*, 92(17) 176403 (2004).
- [17] H.C. Nguyen, J.B. Goodenough, Localized-itinerant electronic transition in the perovskite system La_{1-x}Ca_xVO₃, *Phys. Rev. B*, 52(12), 8776 (1995).
- [18] H.F. Pen, M. Abbate, A. Fujimori, Y. Tokura, H. Eisaki, S. Uchida, and G.A. Sawatzky, Electronic structure of Y_{1-x}Ca_xVO₃ studied by high-energy spectroscopies, *Phys. Rev. B*, 59(11), 7422 (1999).
- [19] T. Schmitt, L.-C. Duda, A. Augustsson, J.-H. Guo, J. Nordgren, J.E. Downes, C. McGuinness, K.E. Smith, G. Dhalenne, A. Revcolevschi, M. Klemm, and Y. Tokura, Resonant soft x-ray emission spectroscopy of V₂O₃, VO₂ and NaV₂O₅, *Surf. Rev. Lett.*, 9, 1369 (2002).
- [20] V. Bisogni, S. Catalano, R.J. Green, M. Gibert, R. Scherwitzl, Y. Huang, V.N. Strocov, P. Zubko, S. Balandeh, J.-M. Triscone, G. Sawtzky, and T. Schmitt, Ground-state oxygen holes and the metal-insulator transition in the negative charge-transfer rare-earth nickelates, *Nat. Comm.*, 7, 13017 (2016).
- [21] J. Laverock, B. Chen, K.E. Smith, R.P. Singh, G. Balakrishnan, M. Gu, J.W. Lu, S.A. Wolf, R.M. Qiao, W. Yang, and J. Adell, Resonant soft x-ray emission as a bulk probe of correlated electron behaviour in metallic Sr_xCa_{1-x}VO₃, *Phys. Rev. Lett.*, 111, 047402 (2013).

- [22] C. Monney, K.J. Zhou, H. Cercellier, Z. Vydrova, M.G. Garnier, G. Monney, V.N. Strocov, H. Berger, H. Beck, T. Schmitt, P. Aebi, Mapping of electron-hole excitations in the charge-density-wave system 1T-TiSe₂ using resonant inelastic x-ray scattering, *Phys. Rev. Lett.*, 109, 047401 (2012).
- [23] R.S. Dhaka, T. Das, N.C. Plumb, Z. Ristic, W. Kong, C.E. Matt, N. Xu, K. Dolui, E. Razzoli, M. Medarde, L. Patthey, M. Shi, M. Radovic, and J. Mesot, Tuning the metal-insulator transition in NdNiO₃ heterostructures via Fermi surface instability and spin fluctuations, *Phys. Rev. B* 92, 035127 (2015).
- [24] J.N. Hancock, R. Viennois, D. Van der Marel, H.M. Ronnow, M. Guarise, P.-H. Lin, M. Grioni, M. Moretti-Sala, G. Ghiringhelli, V.N. Strocov, J. Schlappa, T. Schmitt, Evidence for core-hole-mediated inelastic x-ray scattering from metallic Fe_{1.087}Te, *Phys. Rev. B*, 82, 020513(R) (2010).
- [25] I.H. Inoue, I. Hase, Y. Aiura, A. Fujimori, Y. Haruyama, T. Marayuma, and Y. Nishihara, Systematic development of the spectral function in the 3d1 Mott-Hubbard system Ca_{1-x}Sr_xVO₃, *Phys. Rev. Lett.*, 74(13), 2539 (1995).
- [26] A.S. McLeod, E. van Heumen, J.G. Ramirez, S. Wang, T. Saerbeck, S. Guenon, M. Goldflam, L. Anderegge, P. Kelly, A. Mueller, M.K. Liu, Ivan K. Schuller, and D.N. Basov, Nanotextured phase coexistence in the correlated insulator V₂O₃, *Nat. Phys.*, 13, 80-86 (2017).
- [27] E. Benckiser, L. Fels, G. Ghiringhelli, M. Moretti Sala, T. Schmitt, J. Schlappa, V.N. Strocov, N. Mufti, G.R. Blake, A.A. Nugroho, T.T.M. Palstra, M.W. Haverkort, K. Wohlfeld, and M. Gruninger, Orbital superexchange and crystal field simultaneously at play in YVO₃: Resonant inelastic x-ray scattering at the V L edge and the O K edge, *Phys. Rev. B*, 88, 205115 (2013).

- [28] C. He, T.D. Sanders, M.T. Gray, F.J. Wong, V.V. Mehta, and Y. Suzuki, Metal-insulator transitions in epitaxial LaVO_3 and LaTiO_3 films, *Phys. Rev. B*, 86, 081401(R) (2012).
- [29] S. Beck, G. Sclaurzero, U. Chopra, and C. Ederer, Metal-insulator transition in CaVO_3 thin films: Interplay between epitaxial strain, dimensional confinement, and surface effects, *Phys. Rev. B*, 97, 075107 (2018).
- [30] J. Zaanen, G.A. Sawatzky, and J.W. Allen, Band gaps and electronic structure of transition-metal compounds, *Phys. Rev. Lett.*, 55(4), 418 (1985).
- [31] V.N. Strocov, T. Schmitt, U. Flechsig, T. Schmidt, A. Imhof, Q. Chen, J. Raabe, R. Betemps, D. Zimoch, J. Krempasky, X. Wang, M. Grioni, A. Piazzalunga, and L. Patthey, High-resolution soft X-ray beamline ADRESS at the Swiss Light Source for resonant inelastic X-ray scattering and angle-resolved photoelectron spectroscopies, *J. Synchrotron Rad.*, 17, 631-643 (2010).
- [32] G. Ghiringhelli, A. Piazzalunga, C. Dallera, G. Trezzi, L. Braicovich, T. Schmitt, V.N. Strocov, R. Betemps, L. Patthey, X. Wang, and M. Grioni, SAXES, a high resolution spectrometer for resonant x-ray emission in the 400-1600 eV energy range, *Rev. Sci. Instr.*, 77, 113108 (2006).
- [33] T. Schmitt, V.N. Strocov, K.-J. Zhou, J. Schlappa, C. Monney, U. Flechsig, and L. Patthey, High-resolution inelastic X-ray scattering with soft X-rays at the ADRESS beamline of the Swiss Light Source: Instrumental developments and scientific highlights, *J. Elec. Spec. & Rel. Phen.*, 188, 38-46 (2013).
- [34] M.R. Soman, D.J. Hall, J.H. Tutt, N.J. Murray, A.D. Holland, T. Schmitt, J. Raabe, and B. Schmitt, Developing a CCD camera with high spatial resolution for RIXS in the soft X-ray range, *Nucl. Instrum. Methods Phys. Res. A*, 731, 47 (2013).

Figure Legends:

Figure 1 | Comparison of bandwidth change with cation substitution in bulk $3d^1$ crystals with that realized in thin films of CaVO_3 by reducing film thickness. (a and b) The crystal structure and electronic bandwidth of different $3d^1$ perovskites RXO_3 is presented. For $R = \text{Sr}$ and $X = \text{V}$ a cubic structure is reported. When R is substituted to $R = \text{Ca}$ an orthorhombic distortion occurs changing the electronic bandwidth and local V site symmetry. This results in a more correlated metallic state. When R is substituted to $R = \text{La}$ and X substituted to $X = \text{Ti}$ (to maintain $3d^1$ configuration), the distortion is further increased and a metal-insulator transition occurs (MIT). The MIT is accompanied by long range antiferromagnetic order that can be switched to ferromagnetic by substituting R to $R = \text{Y}$. (c and d) A comparable reduction in bandwidth is found when the MIT in CaVO_3 is controlled by film thickness as described in this manuscript.

Figure 2 | Reduced electronic bandwidth and increased V^{3+} character across the metal-insulator transition in thin film CaVO_3 . (a) Resistance as a function of temperature for the samples indicated. Arrows indicate where the slope of the resistance curve reverses sign for the 15 u.c. and 10 u.c. films. (b) X-ray absorption (XAS) as total fluorescence yield for a CaVO_3 crystal and films with thicknesses as indicated (solid lines) for π -polarised light at a temperature of 20 K. XAS of the 10 u.c. CaVO_3 film at room temperature is shown as a dashed blue curve. Also shown is the XAS for a 50 u.c. SrVO_3 film (dashed black) and VO_2 crystal (dashed grey) and V_2O_3 crystal (dashed magenta).

Figure 3 | Overview of resonant inelastic x-ray scattering (RIXS) measurements across a thickness-induced MIT in vanadate thin films. (top) X-ray absorption total fluorescence yield for samples indicated (a,b,c,d). RIXS intensity maps of energy transfer versus incident energy for

different film thickness across the thickness-induced MIT. CaVO_3 and SrVO_3 metal films are 50 unit cells thick. **(e)** Illustrative sketch of the origin of the Raman and fluorescence peaks measured using RIXS. The sketch is drawn on the total density of states (DOS) and partial DOS for V 3d e_g (red) and V 3d t_{2g} (blue) calculated using density functional theory.

Figure 4 | 40 % bandwidth reduction across the thickness-induced MIT in CaVO_3 thin films. (a,b)

Resonant inelastic x-ray scattering (RIXS) intensity as a function of energy transfer for the films indicated for an incident energy of 520 eV (in the dip between L_3 and L_2 peaks). SrVO_3 and CaVO_3 are 50 u.c. films and also shown are 15 u.c., 10 u.c., 6 u.c. and 4 u.c. CaVO_3 films. All data were recorded at a temperature of 20 K, and normalized to the total integrated intensity and offset by additive constants for clarity except data in (a) that were multiplied by small factors away from unity for clarity. **(c) (top)** V 3d bandwidth of the two features F1 and F2 for different films indicated, as extracted from the data presented in (b); fits for extracting the valence band bandwidth are shown in the supplementary information (S.I.). **(bottom)** Bandwidth and peak position of the electron-hole pair excitations for different films indicated, extracted from the fits shown in S.I. The empty red square, diamond, circle represent bandwidth and peak positions extracted from measurements of the 10 u.c. film in the metallic phase at 300 K presented in Fig. 6.

Figure 5 | Reconstruction of crystal field levels across the thickness-induced MIT. (left)

Resonant inelastic x-ray scattering (RIXS) intensity as a function of energy transfer for the films indicated for an incident energy of 520 eV (in the dip between L_3 and L_2 peaks). SrVO_3 and CaVO_3 are 50 u.c. films and also shown are 15 u.c., 10 u.c., 6 u.c. and 4 u.c. CaVO_3 films. All data were recorded at a temperature of 20 K, and normalized to the total integrated intensity and offset by additive constants for clarity. Labels indicate the different allowed crystal field excitations for V^{4+} and V^{3+}

ions. **(right)** Schematic of the change in the electronic levels of the V 3d electrons due to reconstruction of the local V site environment and valence occupation.

Figure 6 | Resonant inelastic x-ray scattering across the thermal metal-insulator transition in a 10 u.c. CaVO₃ film. (a,b,c,d) Resonant inelastic x-ray scattering (RIXS) intensity as a function of energy transfer at incident photon energy of 520 eV for a 10 u.c. CaVO₃ at 20 K and 300 K. **(inset of a)** Same with elastic line subtracted.

Figures

FIGURE 1

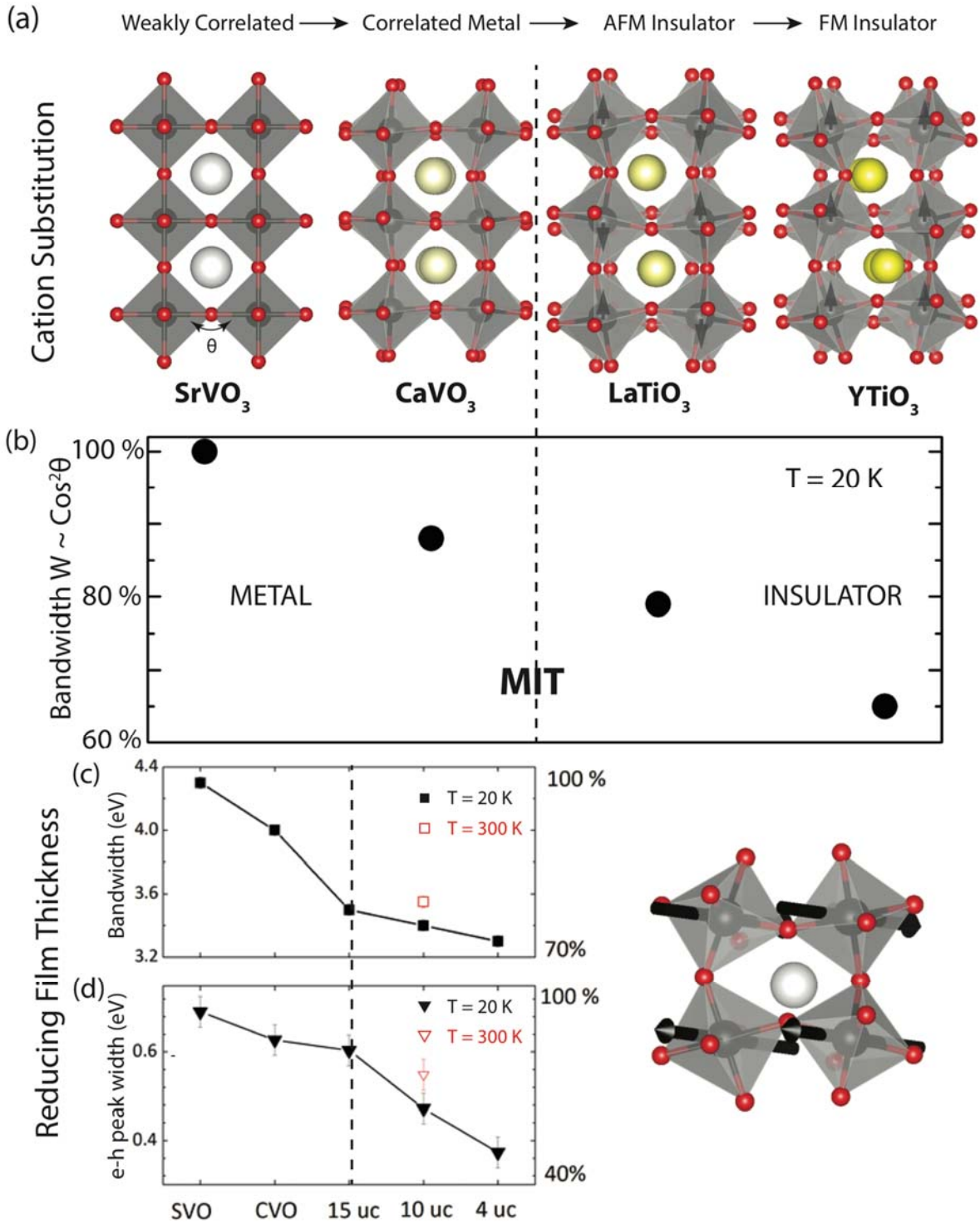


FIGURE 2

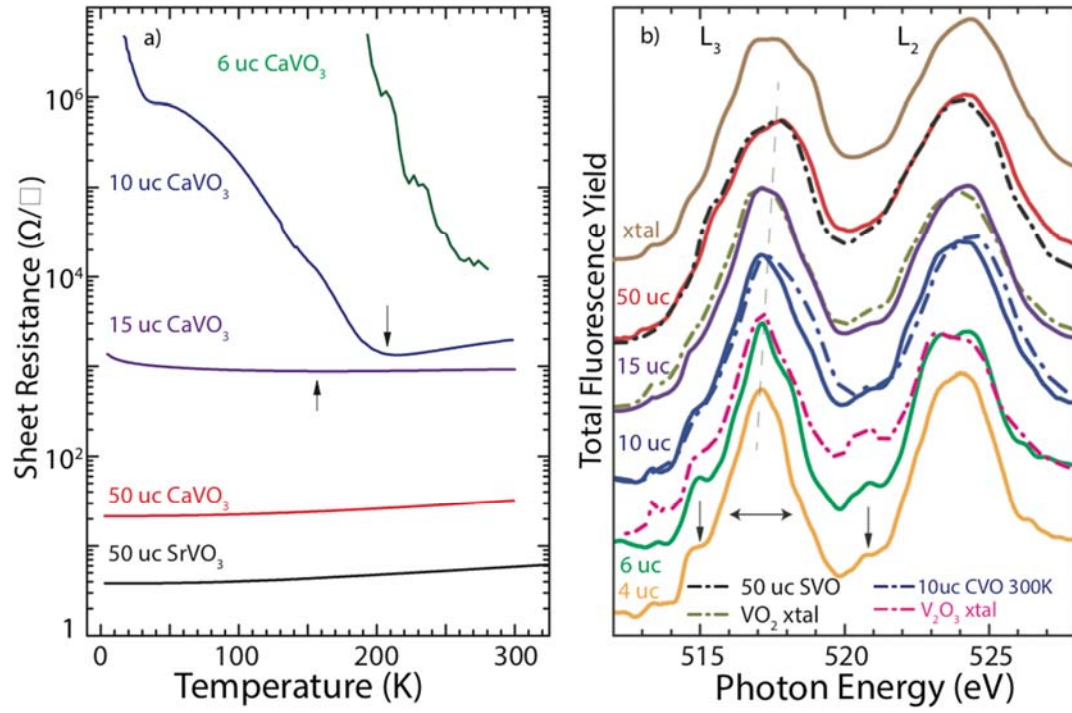


FIGURE 3

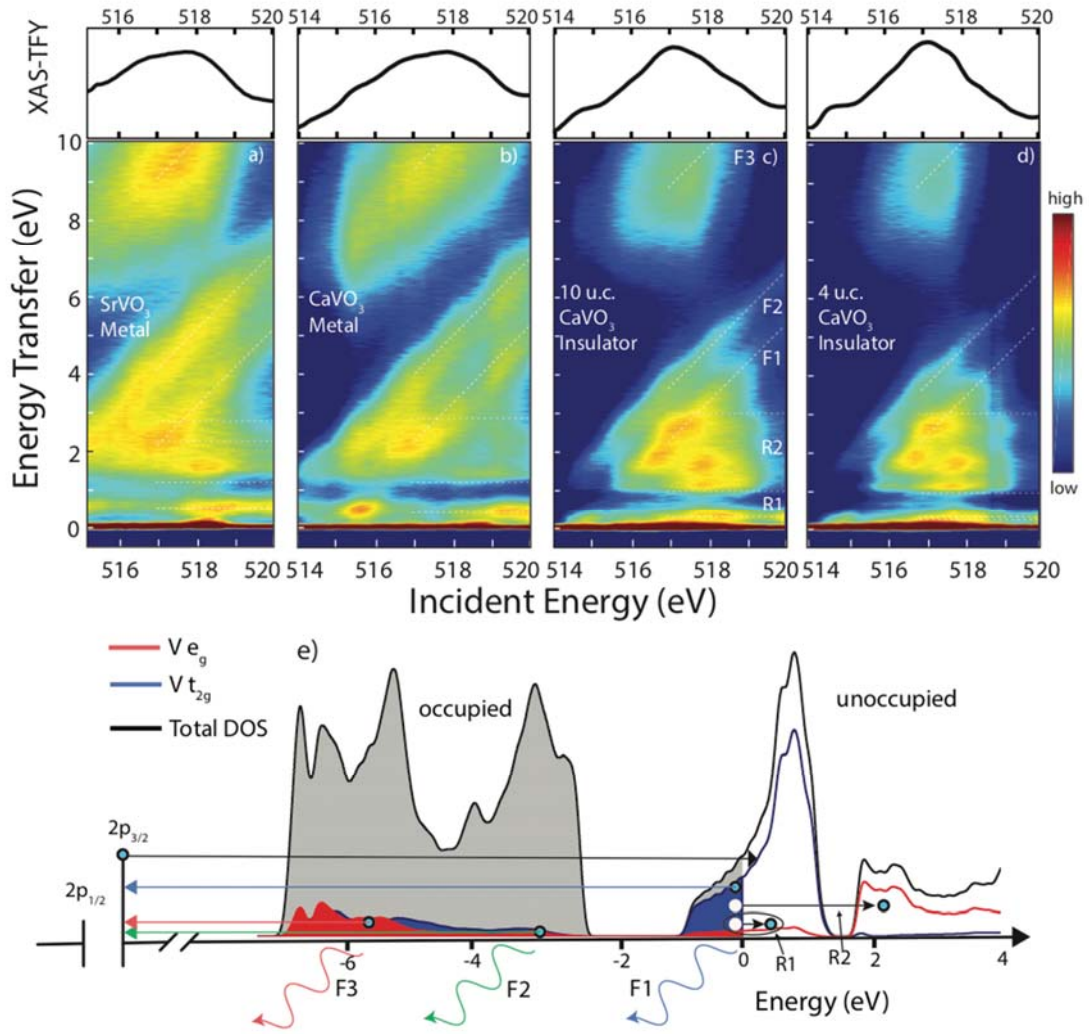


FIGURE 4

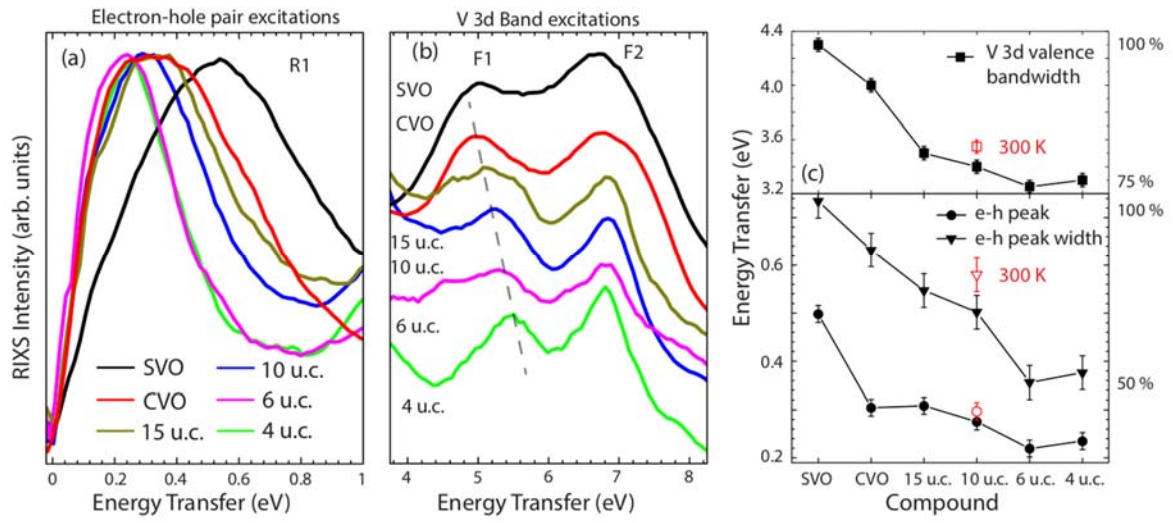


FIGURE 5

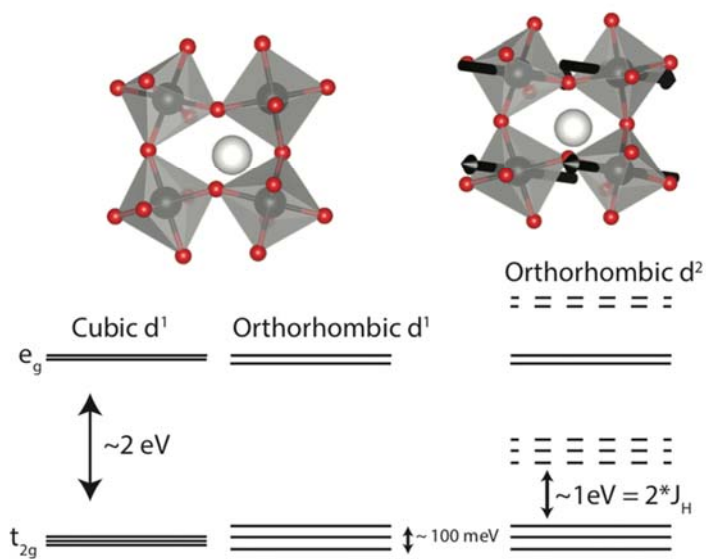
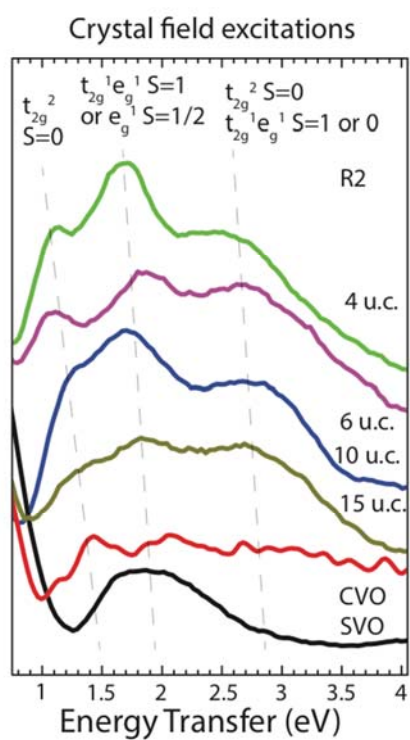


FIGURE 6

